PROCEEDINGS OF SCIENCE

Particle acceleration in superbubbles: MHD simulations and γ-ray signatures

Lucia Härer,[a,*] **Brian Reville,**[a] **Thibault Vieu,**[a] **Jim Hinton,**[a] **Lars Mohrmann**[a] **and Jieshuang Wang**[a]

[a] *Max-Planck-Institut für Kernphysik, Saupfercheckweg 1, 69117 Heidelberg, Germany*

E-mail: lucia.haerer@mpi-hd.mpg.de

An increasing number of star-forming regions and young star clusters are detected in γ-rays, which hints at ongoing particle acceleration. These regions harbour young massive stars, whose powerful winds collectively blow superbubbles (SBs) containing large-scale shocks and tenuous, hot, turbulent plasma. Investigating the physics of SBs is necessary to clarify their role as galactic cosmic ray (CR) sources and their ability to reach energies >1 PeV. In [1], we presented a one-zone emission model for the ring-like H.E.S.S. source surrounding Westerlund 1, a prototypical example for a young massive cluster. The spectrum and the morphology of the source are consistent with a leptonic inverse Compton model, in which the acceleration takes place at the cluster wind termination shock. The ring-like morphology, overall size of the emission region, and energetics disfavour both hadronic models and alternative acceleration sites. Our results showcase the impact of certain environmental parameters on key characteristics of the system. For example, the strength and topology of the magnetic field are critical for the maximum energy, as they affect the acceleration time and particle transport. We briefly summarise the key findings of the Westerlund 1 phenomenological analysis, followed by a report on ongoing work on MHD simulations of star cluster wind.

38th International Cosmic Ray Conference (ICRC2023)
26 July - 3 August, 2023
Nagoya, Japan

*Speaker

PoS(ICRC2023)854

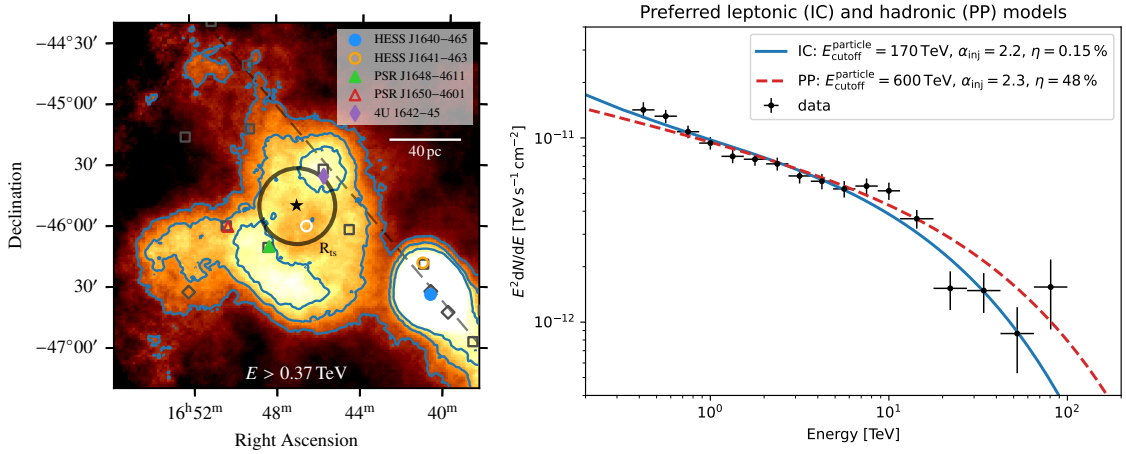

Figure 1: Flux map (left) and SED (right) of HESS J1646−458. Map: adapted from [2], Fig. 1b. The position of Westerlund 1 is marked by a black star. The dark grey circle shows the expected position of the cluster wind termination shock according to [3]. SED: shows the preferred leptonic and hadronic models from [1]. The slope of the particle injection spectrum, its cut-off energy, and the required efficiency[1].

1. Westerlund 1: A leptonic γ-ray source

The number of γ-ray sources associated with young star clusters and star-forming regions has increased significantly (e.g. [4–6]). Wind-blown bubbles around compact, massive clusters in particular are potential sources of Galactic cosmic rays (GCRs) in the PeV range (e.g. [7] and references therein). A recent analysis of H.E.S.S. data revealed ring-like TeV γ-ray emission around Westerlund 1 [2] (designated HESS J1646−458, see Fig. 1), following the detection of the source in 2012 [5]. In previous work [1], we have demonstrated that a predominantly leptonic origin of the emission is preferable. In the following, the two main arguments leading to this conclusion are briefly summarised.

Morphology The morphology is consistent with electron acceleration at the cluster wind termination shock, tracing the inner radius of the γ-ray ring, and subsequent downstream transport within the cooling time. Both advection in the cluster wind and diffusion are found to contribute significantly. For protons, cooling is negligible for the given cluster age. Hence, hadronic models significantly over predict the source size. In addition, the γ-ray emission does not align well with gas maps [2]. In fact, models predict the wind a dense bubble shell at $r \gtrsim 60$ pc, which is expected to be γ-ray bright in the hadronic case, but is not seen.

Energetics The IC model provides a good fit to the spectrum (see Fig. 1). The efficiency[1] is <0.5% for all models across the investigated parameter space. Efficiencies required by hadronic models are much higher, owing to the low density in the wind bubble interior. Extreme ambient densities of $\gtrsim 300\,\mathrm{cm}^{-3}$ or a break not far below the H.E.S.S. band would have to be present. The hadronic model does not include particle escape, which would further exacerbate the efficiency issue.

[1]The efficiency, η, is defined as $L_\gamma(>1\,\mathrm{GeV}) = \eta L_\mathrm{w}$, where $L_\mathrm{w} = 10^{39}\,\mathrm{erg\,s}^{-1}$ is the cluster wind power of Westerlund 1. In other words, η includes both the efficiencies of particle acceleration and γ-ray emission processes.

These arguments do not exclude the presence of a subdominant hadronic component. As the proton cooling time is much longer than the age of the system, hadronic emission could be spread out over a much larger volume, complicating detection.

2. MHD simulations

The work summarised in the preceding section relies on number of simplifying assumptions, due to uncertainty in key parameters. Of particular relevance is the magnetic field, as it impacts the acceleration time, synchrotron cooling, and transport properties. In this section, we report on magneto-hydrodynamic (MHD) simulations of the core of a young massive stellar cluster and its wind bubble. With our setup, we extend previous work covering the core [8] to larger scales. Complementary work using HD simulations is also published in these proceedings [9].

2.1 Setup

We perform 3D ideal MHD simulations on a Cartesian grid, utilising the publicly available code PLUTO[2]. The ambient medium is assumed to be hot (10^4 K) and to be permeated by a uniform 3.5 μG background magnetic field along the x-direction. We consider two cases for the density, $\rho_{\rm amb} = 5\,{\rm cm}^{-3}$ and $100\,{\rm cm}^{-3}$. The density mainly acts as a scaling factor for the size of the wind bubble. We assume an ideal equation of state with an adiabatic index of 5/3. Our cluster setup includes both early-type stars with a fiducial mass-loss of $\dot{M} = 10^{-6}\,{\rm M}_\odot\,{\rm yr}^{-1}$ and terminal wind speed of $v_{\rm w} = 1000\,{\rm km\,s}^{-1}$ and Wolf-Rayet (WR) stars, whose mass-loss is assumed to be enhanced by a factor 100. Two WR setups are used: stationary and intermittent. In the former, WR stars remain active over the full duration of the simulation. In the latter, their positions switch, to study the effects of the additional dynamics compared to the stationary setup. We implement the switch in positions by scaling up early-type winds to WR winds in a subset of stars and selecting a new subset every two 2 kyr. Stellar winds are assumed to be isothermal with $T = 40{,}000$ K. We assume that 10% of the stars have a surface magnetic field, $B_{\rm s} = 1$ kG. This value is consistent with the fraction of so-called magnetic early-type, which have detectable fields in the range of ~100 G–10 kG (e.g. [10]). For the remaining 90% of stars, $B_{\rm s}$ is set to 10 G. In contrast to late-type stars, early-type stars are expected to have regular fields (e.g. [10]), which can be well modelled with a split monopole at the resolution of the simulation. We include a scaling function to smooth the jump at the stellar equator,

$$B_0 = B_{\rm s} \tanh\left(3\left(\frac{\pi}{2} - \theta\right)\right), \tag{1}$$

where θ is the polar angle. Considering stellar rotation, the field has a Parker spiral shape [11],

$$B_{\rm r} = B_0 \frac{{R_*}^2}{r}, \tag{2}$$

$$B_\varphi = B_0 \frac{v_{\rm rot}}{v_{\rm w}} \sin\theta \frac{R_*}{r}\left(1 - \frac{R_*}{r}\right), \tag{3}$$

where $v_{\rm rot}$ is the equatorial rotational velocity and R_* the radius of the star, which are fixed to $100\,{\rm km\,s}^{-1}$ and $16\,R_\odot$, respectively. We use average values instead of a detailed cluster model, since we aim to capture global effects with clearly defined initial assumptions.

[2] http://plutocode.ph.unito.it/

The winds are launched at terminal velocity, flowing out of a spherical region with a radius of five cells, set up as an internal boundary. Inside the boundary, the wind is assumed to be isothermal and its wind density, ρ, follows from mass-continuity,

$$\dot{M} = 4\pi r^2 v_\mathrm{w} \rho(r) \,. \tag{4}$$

The initial conditions outside the boundary are set as follows. Over a radius of ten cells, the density is scaled to ρ_amb. The velocity v_w is then set from Eq. 4. In addition, the pressure and toroidal component of the stellar magnetic field, B_φ, are rescaled such that the sonic and Alfvénic Mach numbers are kept constant. For our fiducial early-type stars and resolution of 0.01 pc per cell, ρ is below ρ_amb at the boundary. As a result v_w and B_φ are scaled down to $\lesssim$10% of their value at the boundary, ensuring a smooth transition into the background. WR wind are assumed to launch into the existing wind profile from an early-type wind and are therefore not treated separately.

The cluster is generated by randomly distributing 50 stars inside a cubic region with 2 pc side length, which we term the cluster core. The orientations of the magnetic axes are also selected randomly. Stars have a minimum central distance of 30 cells, such that the region over which parameters are scaled upon initialisation do not overlap. The simulation box is either limited to the core (see Sect. 2.2), or encompasses a larger region with side length 20 pc (see Sect. 2.3). The latter setup employs a stretched grid with 100 cells each between (-10, -1) pc and (1, 10) pc in the x-, y-, and z-directions. The cluster core is modelled with a uniform grid of 200^3 cells.

2.2 Core simulation

This section discusses a simulation of the cluster core, i.e., the box has a side length of 2 pc. The ambient density is 100 cm^{-3} and WR stars are stationary. All other parameters and settings are as described in Sect. 2.1. Figure 2 shows snapshots of the simulation at 0.6–5 kyr. In the first time-step, individual wind bubbles are still clearly visible, as are the Parker spiral magnetic field structures around individual stars, and the ambient magnetic field along x. The slice also shows the large bubble of a WR star and the slightly deformed bubble of a magnetic early-type star. At consecutive times, the wind bubbles coalesce, creating turbulence, fragmenting the shell, and tangling up the magnetic field. At 5 kyr, a stationary, more ordered flow pattern has emerged, which is dominated by laminar outflows from individual winds. The tangling of field lines appears reduced, in favour of more pronounced spiral structures. Continuing the simulation beyond 5 kyr does not change the flow pattern significantly. Throughout the simulation, magnetic field reach ~500 μG and are highest in regions where winds from magnetic stars get squeezed by WR winds.

2.3 Bubble simulation

For the setup discussed in the preceding section, the cluster core is completely dominated by supersonic outflows after a brief initial period. In this section, we increase the side length of the simulation box to 20 pc, employing a stretched grid as mentioned in Sect. 2.1. The larger box allows us to study the dynamics of the bubble shell, the wind termination shocks, and the post-shock region. This is of particular relevance for the questions raised in Sect. 1.

Figure 3 compares a setup with a high-density, 100 cm^{-3}, ambient medium and stationary WR winds (at 100 kyr, left) to a 5 cm^{-3} case with intermittent WR winds (at 50 kyr, right). These

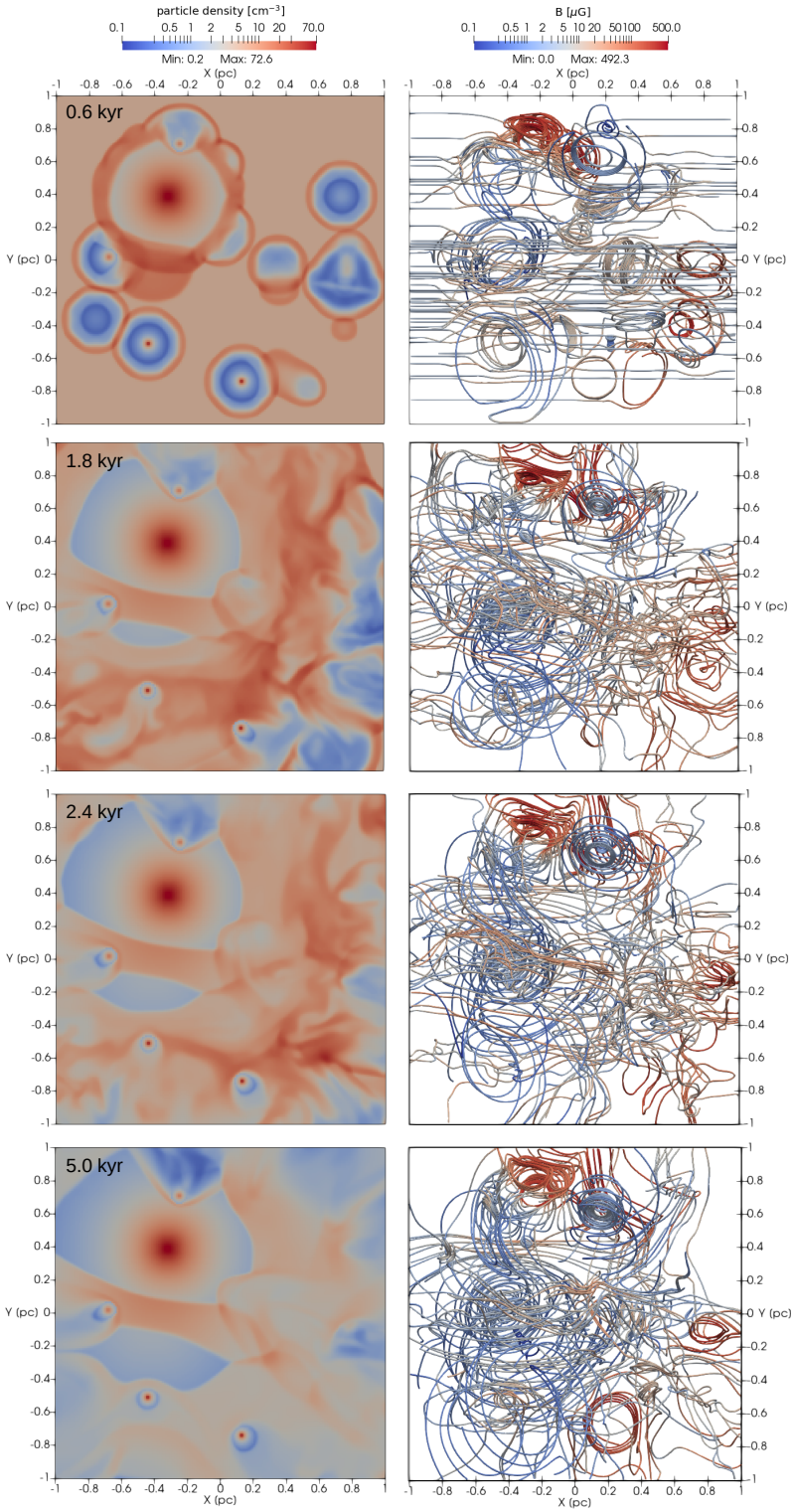

Figure 2: Evolution of the cluster core in the first 5 kyrs, with particle density shown in the left column ($z = 0$ slice) and magnetic field streamlines shown in projection on the right. The ambient density is 5 cm^{-3} and WR positions are stationary. For further details about the setup, see Sect. 2.1.

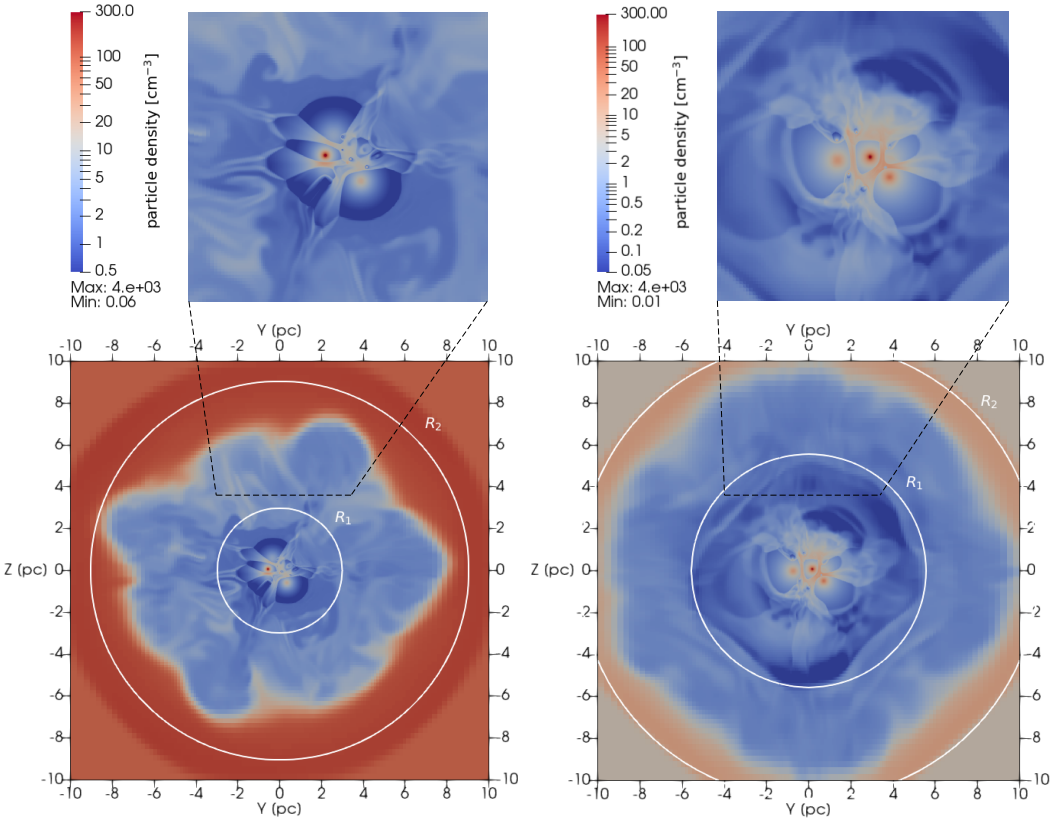

Figure 3: Density slices of the yz-plane, showing the bubble for two cases. Left: after 100 kyr for $\rho_{\rm amb} = 100\,{\rm cm}^{-3}$, and stationary WR winds. Right: after 50 kyr for a particle density of $\rho_{\rm amb} = 5\,{\rm cm}^{-3}$, and intermittent WR winds. White circles represent the radii of the cluster wind termination shock and forward shock predicted by [3]. For more information on the setup, see the text.

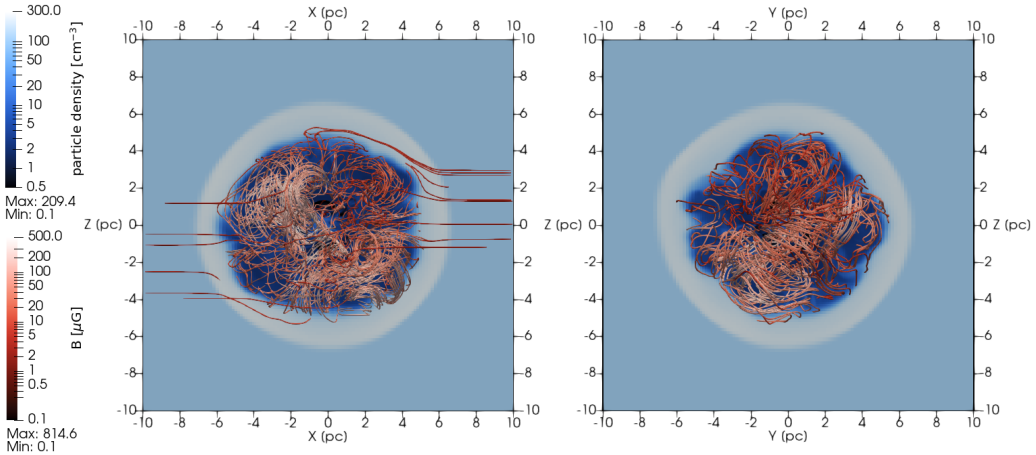

Figure 4: Streamlines of the magnetic field for the stationary WR model (see also Fig. 3, left) after 50 kyr, projected on the xz- (left) and yz-plane (right).

two cases qualitatively highlight parameter dependences. In general, the stationary core observed in the smaller simulation box is recovered. However, the post-termination shock region is found to be highly turbulent and partially filled with material evaporating inwards from the shell. The high-density case shows a thicker shell and higher interior density. The intermittent WR setup generates pocket-like structures surrounding the core.

The white circles in Fig. 3 indicate the positions of the termination shock, R_1, and bubble radius, R_2, predicted by the Weaver model [3], which is an analytic 1D model considering a single central source. While the analytic model recovers R_2 well, R_1 is too large. In the simulation, the individual winds interact to generate turbulent streams flowing out of the core, separating individual stellar termination shocks, which fundamentally differs from the 1D case.

Figure 4 shows magnetic field streamlines for the high-density case, projected onto the xz-plane. The field lines in the bubble interior appear tangled and without significant large-scale structure. The field strength varies and can reach $\gtrsim 100\mu$G.

2.4 Discussion

The simulations recover general features seen in observations and expected from theory, such as the formation of a turbulent post-termination shock region and evaporation at the swept-up shell (for a review see [12]). The cluster core becomes stationary after only ∼5 kyr, while the bubble continues to evolve on a larger scale, displaying complex dynamics in its interior. The core simulation does not capture this dynamics, as shell material is swept out of the box, allowing termination shocks to expand freely, leaving behind mostly supersonic flows. For Westerlund 1, the termination shock is the preferred acceleration site (see [1] and Sect. 1). In this case, full bubble simulations are necessary to investigate the dynamics and physical properties of the shock region relating to particle acceleration.

In interacting the winds in the core, magnetic field strength of up to ∼500 μG were found. Fields of similar scale were found in earlier work [8]. According to [7], such fields are sufficient to allow particle acceleration to PeV energies at supernova shocks expanding in the low-density bubble interior at a high speed.

The results presented in this section are of preliminary nature. The toy-model used for the cluster provides an opportunity for future work, as does the simulated physics. For example, thermal conduction has been shown to have a significant impact in core simulations [8].

3. Conclusion

In this proceeding, we discussed both the leptonic origin of the H.E.S.S. emission surrounding Westerlund 1 and MHD simulations of a young star cluster wind bubble. To assess the role such objects play in the CR ecosystem of the Galaxy and their potential to be PeV γ-ray sources, constraining their physical parameters is crucial. In particular, better constraints can help to the disentangle the hadronic and leptonic components of the γ-ray emission, which is essential to understand the origin of GCRs.

References

[1] L.K. Härer, B. Reville, J. Hinton, L. Mohrmann and T. Vieu, *Understanding the TeV γ -ray emission surrounding the young massive star cluster Westerlund 1*, *Astronomy & Astrophysics* **671** (2023) A4.

[2] F. Aharonian, H. Ashkar, M. Backes, V. Barbosa Martins, Y. Becherini, D. Berge et al., *A deep spectromorphological study of the γ-ray emission surrounding the young massive stellar cluster Westerlund 1*, *A&A* **666** (2022) A124 [2207.10921].

[3] R. Weaver, R. McCray, J. Castor, P. Shapiro and R. Moore, *Interstellar bubbles. II. Structure and evolution.*, *APJ* **218** (1977) 377.

[4] HESS Collaboration, A. Abramowski, F. Acero, F. Aharonian, A.G. Akhperjanian, G. Anton et al., *Revisiting the Westerlund 2 field with the HESS telescope array*, *Astronomy & Astrophysics* **525** (2011) A46.

[5] A. Abramowski, F. Acero, F. Aharonian, A.G. Akhperjanian, G. Anton, S. Balenderan et al., *Probing the extent of the non-thermal emission from the Vela X region at TeV energies with H.E.S.S.*, *A&A* **548** (2012) A38 [1210.1359].

[6] Abramowski, *The exceptionally powerful TeV gamma-ray emitters in the Large Magellanic Cloud*, *Science* **347** (2015) 406.

[7] T. Vieu, B. Reville and F. Aharonian, *Can superbubbles accelerate ultrahigh energy protons?*, *MNRAS* **515** (2022) 2256 [2207.01432].

[8] D.V. Badmaev, A.M. Bykov and M.E. Kalyashova, *Inside the core of a young massive star cluster: 3D MHD simulations*, *Monthly Notices of the Royal Astronomical Society* **517** (2022) 2818.

[9] T. Vieu and B. Reville, *Clustered supernovae as the sources of very-high-energy galactic cosmic rays*, in *38th International Cosmic Ray Conference*, 2023.

[10] J.-F. Donati and J. Landstreet, *Magnetic Fields of Nondegenerate Stars*, *Annual Review of Astronomy and Astrophysics* **47** (2009) 333.

[11] E.N. Parker, *Dynamics of the Interplanetary Gas and Magnetic Fields.*, *The Astrophysical Journal* **128** (1958) 664.

[12] Y.-H. Chu, *Bubbles and Superbubbles: Observations and Theory*, in *IAU Symposium*, vol. 250, pp. 341–354, Proceedings of the International Astronomical Union, 2008, DOI.

PoS(ICRC2023)854